

Convergence of the Born Series with Low-Momentum Interactions

S.K. Bogner¹, R.J. Furnstahl¹, S. Ramanan¹ and A. Schwenk²

¹*Department of Physics, The Ohio State University, Columbus, OH 43210*

²*Department of Physics, University of Washington, Seattle, WA 98195-1560*

Abstract

The nonperturbative nature of nucleon-nucleon interactions as a function of a momentum cutoff is studied using Weinberg eigenvalues as a diagnostic. This investigation extends an earlier study of the perturbative convergence of the Born series to partial waves beyond the 3S_1 - 3D_1 channel and to positive energies. As the cutoff is lowered using renormalization-group or model-space techniques, the evolution of nonperturbative features at large cutoffs from strong short-range repulsion and the iterated tensor interaction are monitored via the complex Weinberg eigenvalues. When all eigenvalues lie within the unit circle, the expansion of the scattering amplitude in terms of the interaction is perturbative, with the magnitude of the largest eigenvalue setting the rate of convergence. Major decreases in the magnitudes of repulsive eigenvalues are observed as the Argonne v_{18} , CD-Bonn or Nijmegen potentials are evolved to low momentum, even though two-body observables are unchanged. For chiral EFT potentials, running the cutoff lower tames the impact of the tensor force and of new nonperturbative features entering at N³LO. The efficacy of separable approximations to nuclear interactions derived from the Weinberg analysis is studied as a function of cutoff, and the connection to inverse scattering is demonstrated.

1 Introduction

Perturbative expansions of the Lippmann-Schwinger equation for the scattering amplitude using conventional nucleon-nucleon interactions fail to converge in low partial waves for several reasons. First is the strongly repulsive short-range interaction present in all conventional potential models, which implies

Email addresses: bogner@mps.ohio-state.edu (S.K. Bogner),
furnstahl.1@osu.edu (R.J. Furnstahl), suna@mps.ohio-state.edu (S.
Ramanan), schwenk@u.washington.edu (A. Schwenk).

large contributions from poorly constrained high-momentum components in intermediate states and requires a nonperturbative treatment. Second is the tensor force, e.g., from pion exchange, which is singular at short distances and requires iteration in the triplet channels. Finally, the presence of low-energy bound states or nearly bound states in the S-waves imply poles in the T matrix that render the perturbative Born series divergent or nearly so. These features greatly complicate the nuclear few- and many-body problems.

However, the nucleon-nucleon potential is not an observable, fixed uniquely from experiment, and these nonperturbative features can vary widely among the infinite number of potentials capable of accurately describing low-energy physics. The effective field theory (EFT) philosophy leads us to exploit this freedom by choosing inter-nucleon interactions appropriate for the physics problem of interest. In this regard, a compelling alternative to conventional potentials for the many-body problem is to use energy-independent nucleon-nucleon interactions with a variable momentum cutoff, which are evolved to low momentum using renormalization-group or model-space methods, together with consistent cutoff-dependent many-nucleon interactions [1,2,3,4,5,6]. These low-momentum potentials, generically called “ $V_{\text{low } k}$ ”, preserve the on-shell T matrix for momenta below the cutoff.¹

Changing the momentum cutoff shifts contributions between nuclear interactions and loop integrals over intermediate states such that two-nucleon observables are unchanged. This affects the perturbativeness of an interaction and the strength of the associated correlations in the wave functions, which means that many-body calculations can be simplified, particularly since Pauli blocking eliminates at moderate densities (well below nuclear matter saturation) the impact of the bound and nearly bound states in the S-waves. In Ref. [5], it was shown that low-momentum interactions make nuclear matter calculations perturbative in the particle-particle channel and that the corresponding low-momentum three-nucleon interactions drive saturation. This refutes the long-standing conventional wisdom that the nuclear matter problem must be nonperturbative in the inter-nucleon interactions in order to obtain saturation.

In order to monitor and quantify our observations about perturbative expansions, a method introduced by Weinberg [9] that focuses on eigenvalues of the operator $G_0(z)V$ proves very useful. This method was applied in Ref. [5] at the deuteron binding energy to the S-waves in free space and in the medium. In the present work, we provide a complete analysis in free space. The Weinberg eigenvalues obtained for nucleon-nucleon interactions are studied as a function of the cutoff for various partial-wave channels and for a range of energies.

¹ In this work, we use $V_{\text{low } k}$ potentials with sharp cutoffs on the relative momenta. The use of smooth cutoffs for $V_{\text{low } k}$, which have technical advantages for some applications, is discussed in Refs. [7,8].

When these complex eigenvalues lie within the unit circle, the T matrix expansion in terms of the potential V is perturbative, and the largest eigenvalue determines the rate of convergence. By focusing separately on the “attractive” and “repulsive” eigenvalues (see Sect. 2), we can isolate the different sources of nonperturbative behavior in nuclear forces.

In Sect. 2, we apply this analysis to $V_{\text{low } k}$ derived from the Argonne v_{18} potential [10], which has been used in the most accurate ab-initio calculations of nuclei and nuclear matter to date. The removal of the strongly repulsive core with decreasing cutoff is tracked quantitatively via the largest repulsive Weinberg eigenvalues. Comparisons to other potentials (CD-Bonn [11] and Nijmegen [12]) shows the model dependence inherent in the short-distance descriptions, which is removed as the cutoff is lowered to 2 fm^{-1} . Chiral EFT potentials [13,14], which provide a more systematic and model-independent approach to inter-nucleon interactions, typically have cutoffs below 3.5 fm^{-1} , but running the cutoff lower tames the impact of the tensor force and of new nonperturbative features entering at N^3LO . The eigenvectors corresponding to the Weinberg eigenvalues lead naturally to separable approximations to the nucleon-nucleon interaction [15]. In Sect. 3, we show that the expansion in separable potentials becomes more effective for lower cutoffs, and compare $V_{\text{low } k}$ with separable inverse-scattering solutions. Sect. 4 summarizes our conclusions.

2 Weinberg Eigenvalue Analysis for Low-Momentum Interactions

The eigenvalue analysis introduced by Weinberg [9] provides quantitative conditions for the perturbative convergence of the T matrix. This allows us to identify momentum cutoffs at which repulsive core scattering and iterated tensor contributions become perturbative. Here we briefly review the Weinberg formalism and refer the reader to the literature [9,15,16,17] for more details.

The Lippmann-Schwinger equation for the T matrix with energy-independent potential V is given in operator form by

$$T(z) = V + VG_0(z)T(z), \quad (1)$$

where the free propagator $G_0(z)$ with kinetic energy H_0 is

$$G_0(z) = \frac{1}{z - H_0}. \quad (2)$$

The T matrix can be expanded in the perturbative Born series as

$$T(z) = V + VG_0(z)V + VG_0(z)VG_0(z)V + \dots \quad (3)$$

We are interested in the convergence of this series at different energies, which is closely related to the presence of bound states or resonances. Suppose that V supports a bound state at $z = E_b < 0$. Since $T(z)$ has a pole at $z = E_b$ and the individual terms in the Born series are all finite, this implies that the series diverges as $z \rightarrow E_b$.

We can rewrite the eigenvalue problem for the bound state $|b\rangle$,

$$(H_0 + V)|b\rangle = E_b|b\rangle, \quad (4)$$

as

$$\frac{1}{E_b - H_0}V|b\rangle = G_0(E_b)V|b\rangle = |b\rangle, \quad (5)$$

which motivates the generalization to a new eigenvalue problem for complex energies z :

$$G_0(z)V|\Psi_\nu(z)\rangle = \eta_\nu(z)|\Psi_\nu(z)\rangle. \quad (6)$$

Here the index ν labels the Weinberg eigenvalues (which are always discrete [9,17]) and eigenvectors. The $\eta_\nu(z)$ are analytic functions cut along $0 \leq z < \infty$ [17]. For positive energies, the eigenvalues are defined as the limits on the upper or lower edges of the cut:

$$\lim_{\epsilon \rightarrow 0} G_0(E \pm i\epsilon)V|\Psi_\nu^{(\pm)}(E)\rangle = \eta_\nu^{(\pm)}(E)|\Psi_\nu^{(\pm)}(E)\rangle. \quad (7)$$

In the following, it is understood that for positive energy $\eta_\nu(E) = \eta_\nu^{(+)}(E)$.

As demonstrated in Ref. [9], the perturbative Born series for $T(z)$ diverges if and only if there is an eigenvalue with $|\eta_\nu(z)| \geq 1$. The necessity of this condition is clear, since

$$T(z)|\Psi_\nu(z)\rangle = \left(1 + \eta_\nu(z) + \eta_\nu(z)^2 + \dots\right)V|\Psi_\nu(z)\rangle \quad (8)$$

diverges for $|\eta_\nu(z)| \geq 1$. Any scattering state $|\Psi\rangle$ can be written as a linear combination of the Weinberg states $|\Psi_\nu(z)\rangle$, thus the Born series will converge only if all $\eta_\nu(z)$ lie within the unit circle. Furthermore, the rate of convergence is controlled by the largest $|\eta_\nu(z)|$, with smaller magnitudes implying faster convergence.

A rearrangement of Eq. (6) gives a simple interpretation of the eigenvalues $\eta_\nu(z)$ in terms of the Schrödinger equation,

$$\left(H_0 + \frac{1}{\eta_\nu(z)}V\right)|\Psi_\nu(z)\rangle = z|\Psi_\nu(z)\rangle. \quad (9)$$

The eigenvalue $\eta_\nu(z)$ can thus be viewed as an energy-dependent coupling that must divide V to produce a solution to the Schrödinger equation at energy z . If V supports a bound state at $z = E_B$, then there is some ν with $\eta_\nu(E_B) = 1$, which implies a divergence of the Born series for nearby energies. However,

what matters for convergence at a given energy z is not simply the presence of nearby physical bound states, but rather the entire set of eigenstates that can be shifted to z when the interaction is divided by $\eta_\nu(z)$. For negative energies, a purely attractive V gives positive $\eta_\nu(z)$ values, while a purely repulsive V gives negative eigenvalues, as the sign of the interaction must be flipped to support a bound state. For this reason, we follow convention and refer to negative eigenvalues as repulsive and positive ones as attractive. In the case of conventional nuclear interactions, the repulsive core generates at least one large and negative eigenvalue that causes the Born series to diverge in the low partial waves.

For energies greater than zero, the eigenvalues are still discrete but become complex. Weinberg also showed that there are at most a finite number of eigenvalues with magnitudes greater than unity [9]. This is used in Weinberg’s “quasiparticle” method to systematically isolate the nonperturbative parts of the potential in separable form. The eigenvalues vary continuously with energy, so they can be plotted as trajectories in the complex plane, as in Figs. 1 and 2. For each energy, the overall largest eigenvalue determines whether or not the Born series converges at that energy. But by considering attractive and repulsive eigenvalues separately we can isolate the contributions of different sources of nonperturbative behavior.

Here we calculate the Weinberg eigenvalues in different partial waves as a function of energy for $V_{\text{low } k}$ over a wide range of cutoffs. The construction of $V_{\text{low } k}$ using renormalization-group (RG) or model-space methods is described in detail elsewhere [2,3]. In short, the RG approach starts with the partial-wave Lippman-Schwinger equation for the T matrix with a cutoff Λ on intermediate relative momenta. By imposing the condition $dT(k', k; k^2)/d\Lambda = 0$ on the half-on-shell T matrix, we ensure that low-momentum observables are independent of the scale Λ and generate energy-independent potentials. This leads to coupled differential equations for the interaction $V_{\text{low } k}(k', k)$, which are solved on a momentum grid suitable for Gaussian integration, starting from a large initial Λ_0 appropriate for the starting “bare” interaction. This starting point could be the Argonne v_{18} , CD-Bonn, or Nijmegen potential, the chiral EFT potentials at N³LO, or any other potential that reproduces two-body observables. For sharp cutoffs $\Lambda \geq 2 \text{ fm}^{-1}$, the resulting $V_{\text{low } k}$ preserves the elastic phase shifts up to laboratory energies $E_{\text{lab}} = 2\Lambda^2 \geq 330 \text{ MeV}$ (in units where $\hbar^2/m = 1$). $V_{\text{low } k}(k', k)$ is obtained on a momentum grid, where the eigenvalue problem Eq. (6) is given by

$$\frac{2}{\pi} \int_0^\Lambda k^2 dk \frac{V_{\text{low } k}(k', k)}{p^2 - k'^2 + i\epsilon} \langle k | \Psi_\nu(p^2) \rangle = \eta_\nu(p^2) \langle k' | \Psi_\nu(p^2) \rangle. \quad (10)$$

We solve Eq. (10) by converting it to a left-eigenvalue problem, where we integrate over the singularity using $1/(x + i\epsilon) = \mathcal{P}/x - i\pi\delta(x)$. Alternatively,

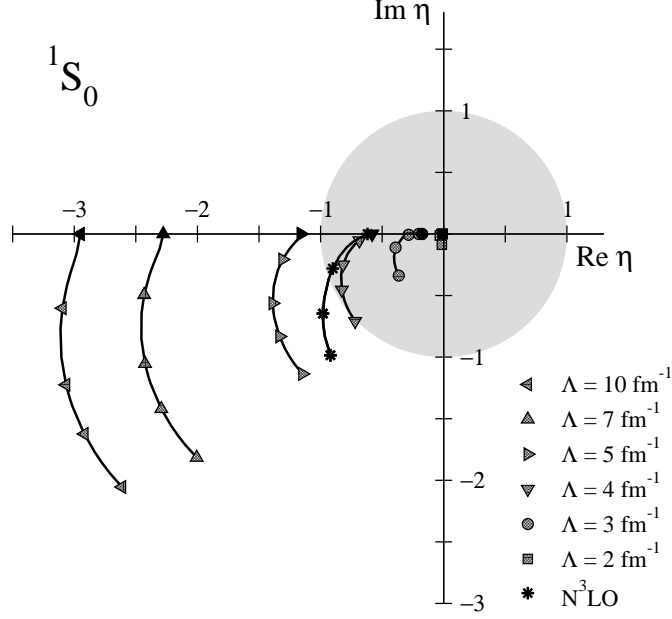


Fig. 1. Trajectories of the largest repulsive Weinberg eigenvalue in the 1S_0 channel as a function of energy for $V_{\text{low } k}$ derived from the Argonne v_{18} potential. Our results for selected cutoffs are indicated by the different symbols. The positions of the symbols on each trajectory mark the eigenvalues for center-of-mass energies $E_{\text{cm}} = k^2 = 0, 25, 66, 100$ and 150 MeV, starting from the filled symbol at 0 MeV. The trajectory with stars are eigenvalues for the $N^3\text{LO}$ potential of Ref. [13].

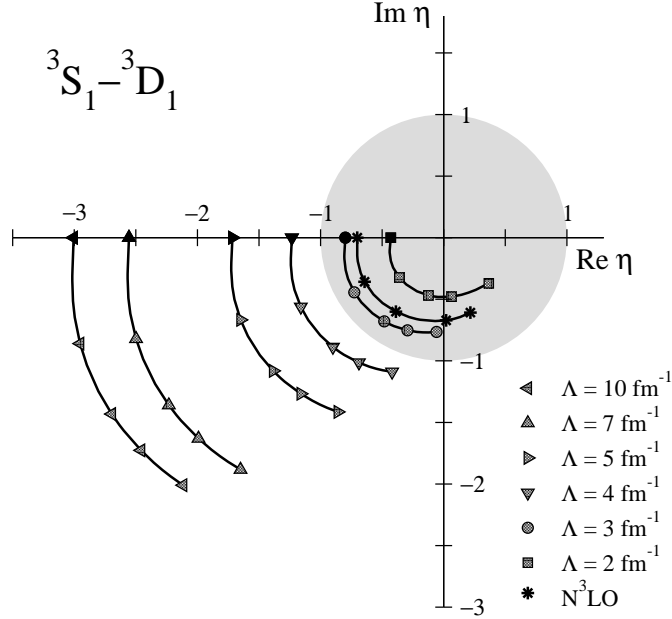


Fig. 2. Trajectories of the largest repulsive Weinberg eigenvalue in the 3S_1 - 3D_1 coupled channel as a function of energy for $V_{\text{low } k}$ derived from the Argonne v_{18} potential. Our results for selected cutoffs are indicated by the different symbols. The positions of the symbols on each trajectory mark the eigenvalues for center-of-mass energies $E_{\text{cm}} = 0, 25, 66, 100$ and 150 MeV, starting from the filled symbol at 0 MeV. The trajectory with stars are eigenvalues for the $N^3\text{LO}$ potential of Ref. [13].

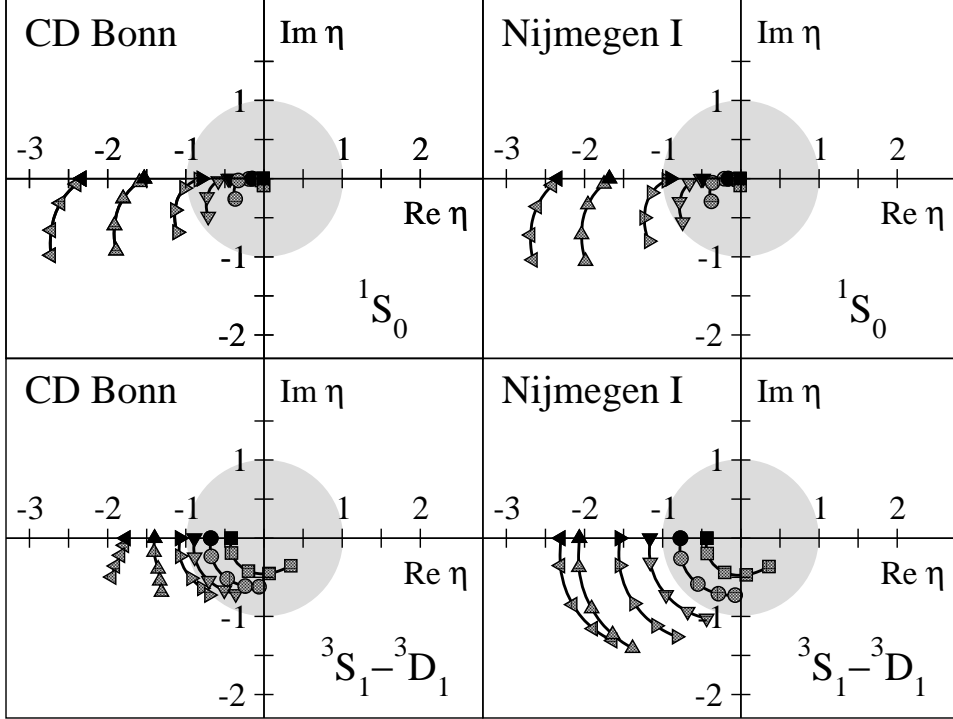


Fig. 3. Trajectories of the largest repulsive Weinberg eigenvalue in the 1S_0 channel and the $^3S_1-^3D_1$ coupled channel as a function of energy for $V_{\text{low } k}$ derived from the CD-Bonn (left) and Nijmegen I potentials (right). Our results for selected cutoffs are indicated by the different symbols (see Fig. 1 for the legend). The positions of the symbols on each trajectory mark the eigenvalues for center-of-mass energies $E_{\text{cm}} = 0, 25, 66, 100$ and 150 MeV, starting from the filled symbol at 0 MeV.

we can solve the complex right-eigenvalue problem for $VG_0(z)[V|\Psi_\nu(z)\rangle] = \eta_\nu(z)[V|\Psi_\nu(z)\rangle]$, which has the same spectrum as $G_0(z)V$ and integrates over the singularity directly.

In Figs. 1 and 2, we show the trajectories of the largest repulsive eigenvalue for the S-waves as a function of positive energy over a range of cutoffs from $\Lambda = 10 \text{ fm}^{-1}$ to 2 fm^{-1} . The eigenvalues are for the $V_{\text{low } k}$ evolved from the Argonne v_{18} potential, and for $\Lambda > 10 \text{ fm}^{-1}$ there are essentially no changes in the eigenvalues. In all cases, a trajectory starts on the real axis with energy $E = 0$ (for repulsive eigenvalues $\eta_\nu(0) < 0$) and evolves counter-clockwise [9]. If E were decreased to negative values, the trajectory would continue along the real axis with decreasing magnitude of η as E becomes more negative. It is evident that the magnitude of the largest repulsive eigenvalue at all energies is greatly cutoff dependent. The decrease with lowering the cutoff reflects the elimination of the repulsive core of the potential. In the singlet channel, Fig. 1, the trajectory lies completely inside the shaded unit circle for cutoffs near 4 fm^{-1} and below, which implies that the Born series becomes perturbative with respect to the repulsive core (but still converges very slowly at low energies due to the nearly bound state at threshold, see the discussion

on the attractive Weinberg eigenvalue and Fig. 8 below). By $\Lambda = 2 \text{ fm}^{-1}$ the largest repulsive eigenvalue is very small at all energies, which shows that the nonperturbative behavior from the repulsive core has been eliminated and has little impact on the convergence.

In the triplet channel, Fig. 2, where the tensor contribution is active, the repulsive core is still the dominant source for the largest repulsive eigenvalue. When the cutoff is lowered to eliminate the core, the repulsive tensor interaction is left as the now-dominant feature in the triplet channel, so that the largest repulsive eigenvalues are just within the unit circle for $\Lambda = 3 \text{ fm}^{-1}$ and still have a magnitude of $\eta \approx 0.5$ for $\Lambda = 2 \text{ fm}^{-1}$. However, the decrease from $\Lambda = 3 \text{ fm}^{-1}$ to 2 fm^{-1} is significant for ensuring a convergence of particle-particle ladders in the nuclear medium, since second-order tensor contributions are known to strongly excite intermediate-state momenta peaked at $k \approx 2.5 - 3.5 \text{ fm}^{-1}$ in nuclear matter [18]. In Fig. 3 we show the largest repulsive Weinberg eigenvalues of $V_{\text{low } k}$ obtained from the CD-Bonn and Nijmegen I potentials. The eigenvalues for these energies are nearly identical for cutoffs below $\Lambda = 3 \text{ fm}^{-1}$, whereas the coalescence of all momentum-space matrix elements of $V_{\text{low } k}$ occurs for lower cutoffs $\Lambda \sim 2 \text{ fm}^{-1}$ [1,2]. We further observe that the singlet channel eigenvalues are very similar even for larger cutoffs, but the triplet eigenvalues differ substantially for large cutoff.

Chiral EFT interactions typically have cutoffs below 3.5 fm^{-1} and therefore are expected to be soft potentials. However, as shown in Fig. 1, the N³LO potential of Entem and Machleidt [13] has substantial repulsive eigenvalues in the singlet channel, which are close to the $V_{\text{low } k}$ results for $\Lambda = 4 \text{ fm}^{-1}$. Therefore, we study the behavior of chiral EFT interactions in more detail in Figs. 4 and 5, using Weinberg eigenvalues as a diagnostic. Our results show that the repulsive eigenvalues are large for the N³LO potential of Epelbaum *et al.* [14], and that there is a major decrease as the cutoff is run down from $\Lambda = 3 \text{ fm}^{-1}$ to 2 fm^{-1} . This decrease is important, as the magnitude of the largest repulsive eigenvalue increases in the ¹S₀ channel for $E > 0$ (see Fig. 1) and because the tensor force in the ³S₁–³D₁ coupled channel is softened when chiral interactions are evolved to lower cutoffs (see also Fig. 2).

In addition to the tensor contribution at all orders, there are new nonperturbative sources due to the central parts of pion exchanges that enter at N³LO. This can be seen from the S-wave component of the deuteron wave function at N³LO, Fig. 13 in Ref. [14], where the very short-range part for $\Lambda = 550 \text{ MeV}$ is similar to what is found with a repulsive core (even for $\Lambda = 450 \text{ MeV}$, the S-wave deuteron wave function lies between the bare Argonne v_{18} potential and $V_{\text{low } k}$ for $\Lambda = 4 \text{ fm}^{-1}$). This observation and the comparison in Fig. 4 to the eigenvalues of the N²LO potential [19] suggest that the large repulsive Weinberg eigenvalues at N³LO are due to nonperturbative features in the central part of the sub-sub-leading 2π -exchange interaction. This might

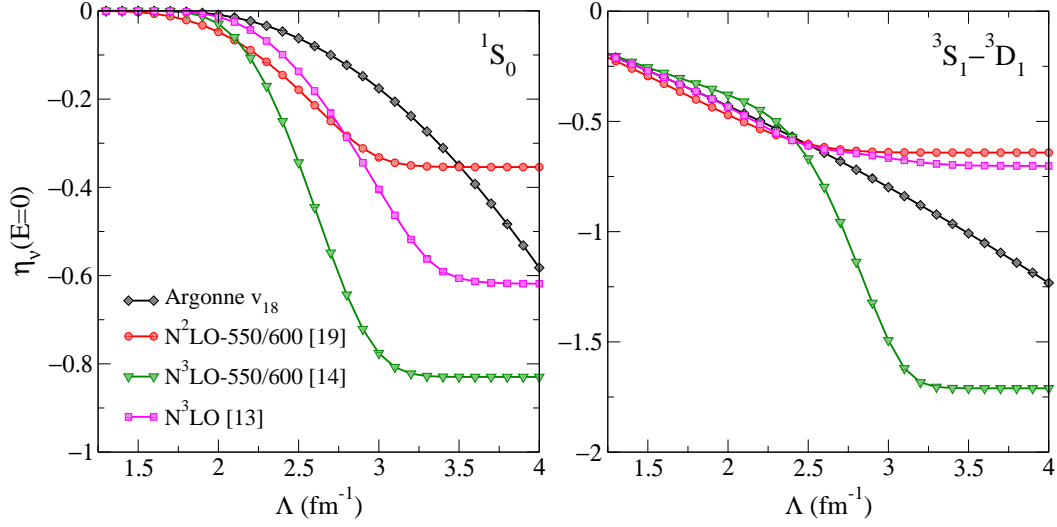


Fig. 4. The largest repulsive Weinberg eigenvalues for $E = 0$ in the 1S_0 channel (left) and the 3S_1 - 3D_1 coupled channel (right) as a function of cutoff for $V_{\text{low } k}$ derived from chiral interactions. Results are shown for the $N^3\text{LO}$ potential of Entem and Machleidt [13], for the $N^3\text{LO}$ potential of Epelbaum *et al.* [14] with different cutoffs $\Lambda/\bar{\Lambda}$ (as indicated in MeV), and for the $N^2\text{LO}$ potential [19]. For comparison, we have plotted the largest repulsive Weinberg eigenvalues for $V_{\text{low } k}$ derived from the Argonne v_{18} potential.

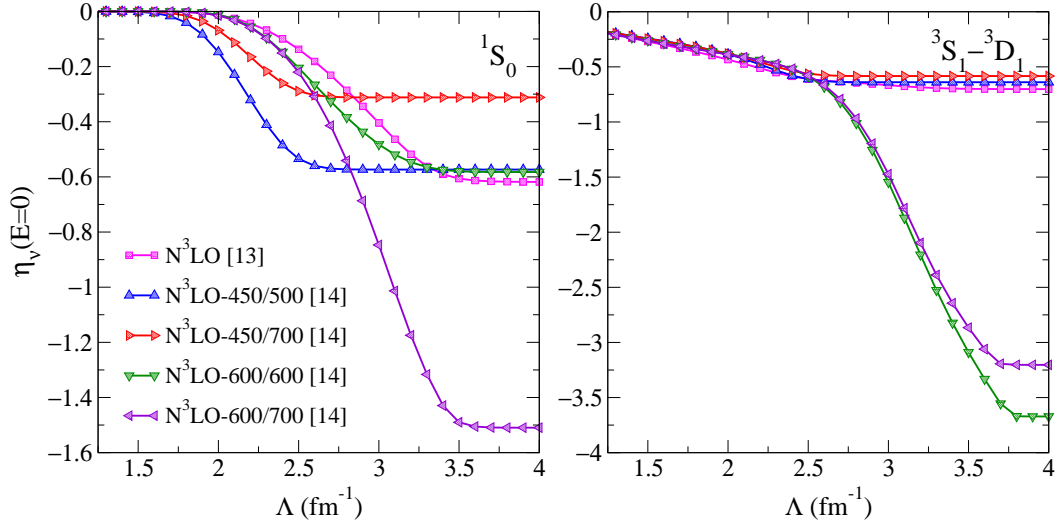


Fig. 5. The largest repulsive Weinberg eigenvalues for $E = 0$ in the 1S_0 channel (left) and the 3S_1 - 3D_1 coupled channel (right) as a function of cutoff for $V_{\text{low } k}$ derived from chiral interactions. Results are shown for the $N^3\text{LO}$ potential of Entem and Machleidt [13] and for the $N^3\text{LO}$ potential of Epelbaum *et al.* [14] with different cutoffs $\Lambda/\bar{\Lambda}$ (as indicated in MeV).

be understood from the short-distance behavior of the isoscalar central 2π -exchange two-loop contributions, discussed in [20]. The repulsive eigenvalues of the N³LO potential of Entem and Machleidt [13], which uses $\Lambda = 500$ MeV, are smaller and close to the $\Lambda = 450$ MeV N³LO potentials of Epelbaum *et al.* [14]. The differences in implementation between [13] and [14], such as the fitting of low-energy constants and the regularization of two-pion exchange at N³LO are reflected in the eigenvalues. As seen in Fig. 5, however, the patterns of eigenvalues are not completely systematic and require further study, which is deferred to a future publication. In any case, Figs. 4 and 5 clearly show that it is advantageous to evolve chiral EFT interactions to lower cutoffs using the RG, since the singular central (at N³LO) and the singular tensor parts are softened for lower cutoffs.

In Figs. 6 and 7, the magnitudes of the largest repulsive eigenvalues for the Argonne v_{18} potential are shown for a set of representative partial waves. The results are plotted as a function of energy for selected cutoffs and as a function of cutoff for selected energies, respectively (where not plotted, the eigenvalue was too small in magnitude to unambiguously identify). The same monotonic decrease in magnitude with decreasing cutoff is seen in every channel. The crossover from the nonperturbative ($|\eta| > 1$) to the perturbative regime ($|\eta| < 1$) happens at different cutoffs in different channels, but always for $\Lambda > 3 \text{ fm}^{-1}$. For completeness, we note that the second-largest repulsive eigenvalue is below unit magnitude in all channels for all cutoffs, but shows the same rapid decrease to very small values by $\Lambda = 2 \text{ fm}^{-1}$.

Next, we study the largest attractive Weinberg eigenvalues. Their trajectories for the S-waves are plotted as a function of energy in Figs. 8 and 9. The values $\eta(E = 0) \approx 1$ reflect the presence of a bound state close to zero energy; if the potential were scaled in each case to $V/\eta(0)$, there would be a bound state exactly at zero energy. Conversely, all nuclear interactions have a unit eigenvalue $\eta(E_d) = 1$ in the triplet channel, corresponding to the deuteron binding energy $E_d = -2.225$ MeV. We find that the attractive eigenvalues increase insubstantially in magnitude as Λ decreases. This small increase is similar for all energies. As expected, the eigenvalue close to unit magnitude persists as we lower the cutoff. This is because it is dictated by physics, namely the near-zero-energy bound states. However, we have shown in Ref. [5] that the large attractive eigenvalues decrease rapidly as a function of density due to Pauli blocking. In contrast, the large repulsive eigenvalues for large cutoffs are little affected by Pauli blocking.

The role of the tensor force can be seen by comparing the 3P_0 and 3P_1 channels in Figs. 7 and 10. The comparison shows similar repulsive eigenvalues (in magnitude) at large cutoff, where the dominant effect is the short-range repulsion. At the smallest cutoffs, 3P_0 has tiny repulsive eigenvalues while the 3P_1 repulsive eigenvalues are non-negligible. This is consistent with tensor contri-

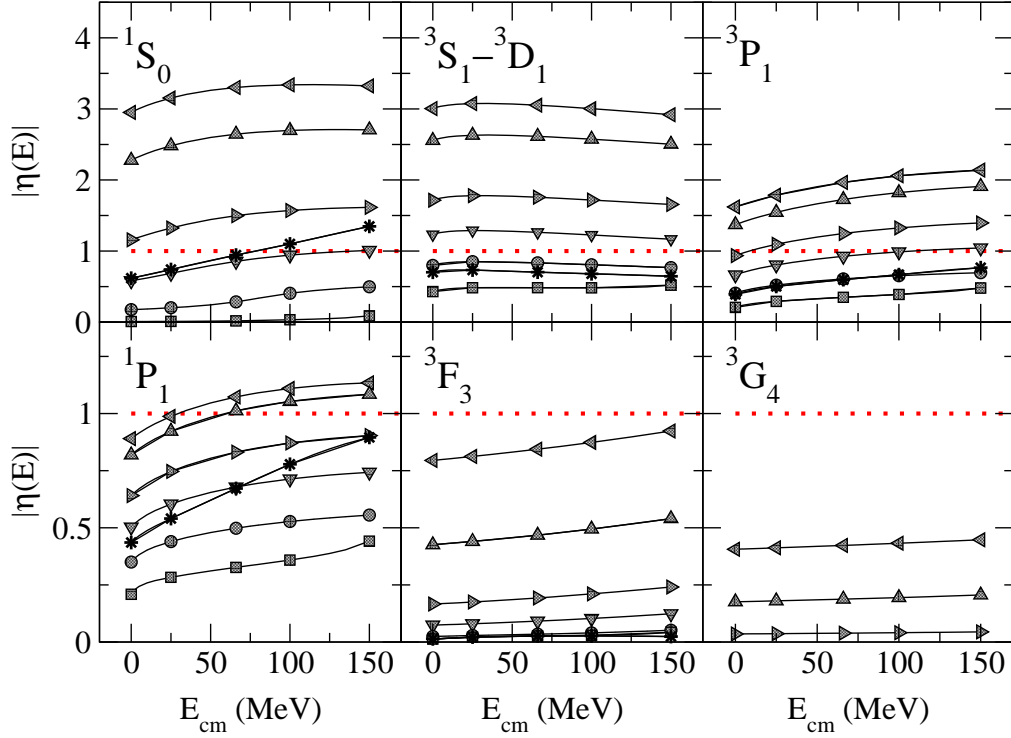


Fig. 6. The magnitude of the largest repulsive Weinberg eigenvalue as a function of center-of-mass energy E_{cm} in selected channels for a range of cutoffs. The symbols label the same cutoffs and the $N^3\text{LO}$ potential [13] as in Fig. 1.

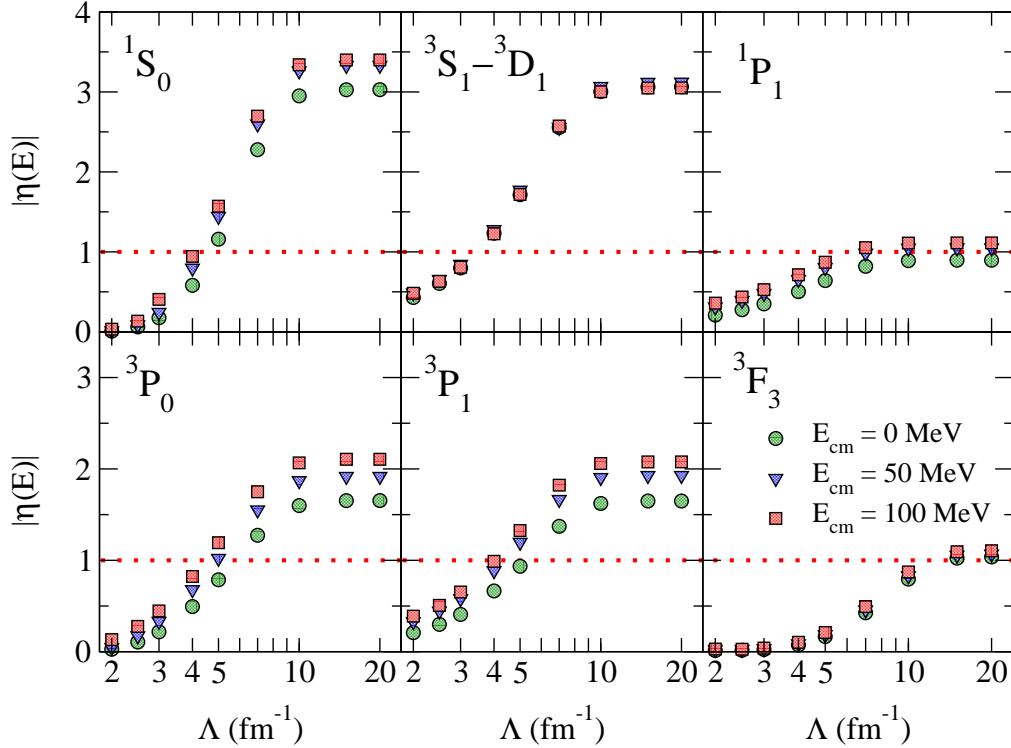


Fig. 7. The magnitude of the largest repulsive Weinberg eigenvalue as a function of cutoff Λ in selected channels for three center-of-mass energies.

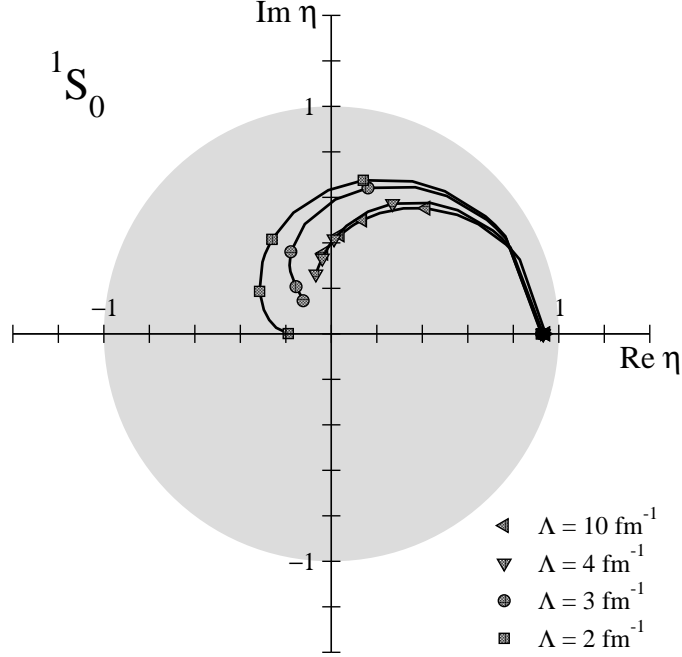


Fig. 8. Trajectories of the largest attractive Weinberg eigenvalue in the 1S_0 channel as a function of energy for $V_{\text{low}k}$ derived from the Argonne v_{18} potential. Our results for selected cutoffs are indicated by the different symbols. The positions of the symbols on each trajectory mark the eigenvalues for center-of-mass energies $E_{\text{cm}} = 0, 25, 66, 100$ and 150 MeV, starting from the filled symbol at 0 MeV.

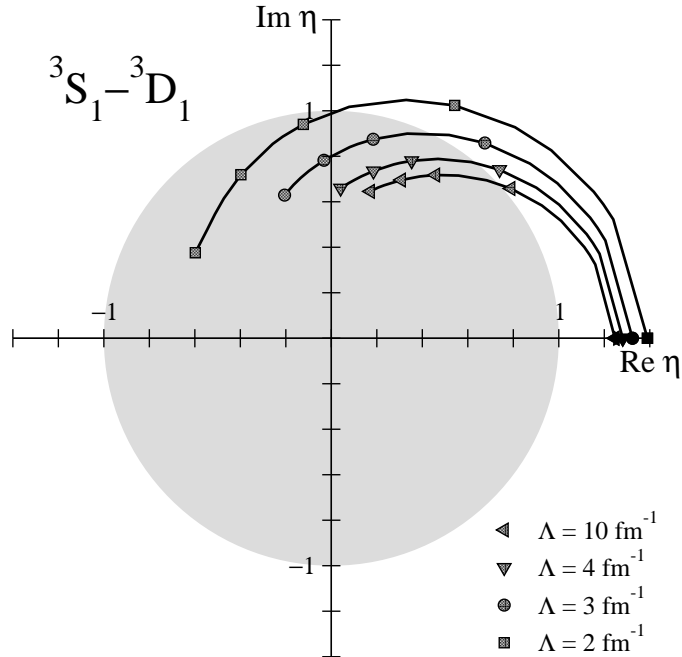


Fig. 9. Trajectories of the largest attractive Weinberg eigenvalue in the 3S_1 - 3D_1 coupled channel as a function of energy for $V_{\text{low}k}$ derived from the Argonne v_{18} potential. Our results for selected cutoffs are indicated by the different symbols. The positions of the symbols on each trajectory mark the eigenvalues for center-of-mass energies $E_{\text{cm}} = 0, 25, 66, 100$ and 150 MeV, starting from the filled symbol at 0 MeV.

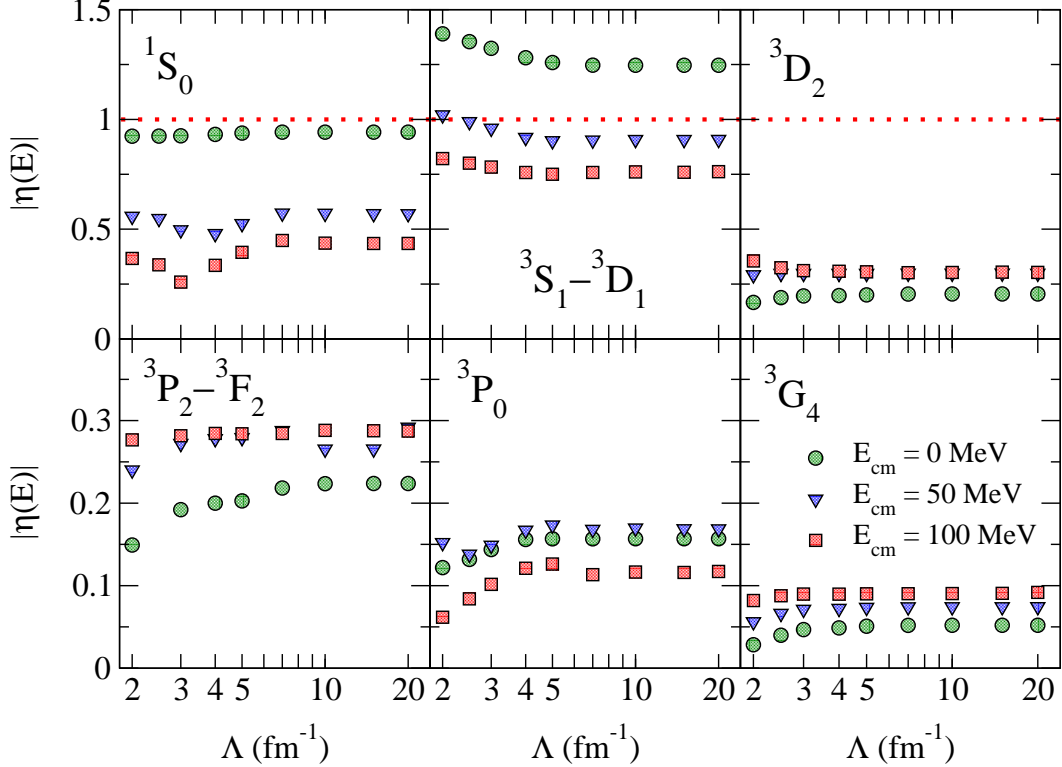


Fig. 10. The magnitude of the largest attractive Weinberg eigenvalue as a function of Λ in selected channels for three laboratory energies. There are no significant attractive Weinberg eigenvalues for any Λ in the 1P_1 , 3P_1 and 3F_3 channels and where not plotted, the eigenvalue was too small in magnitude to unambiguously identify.

butions being attractive in 3P_0 and repulsive in 3P_1 . Figure 10 shows that the largest attractive eigenvalues for channels besides the S-waves are where the long-range one-pion exchange tensor force is attractive (3P_0 , 3P_2 - 3F_2 , 3D_2 and 3G_4). The eigenvalues in the channels not shown are very small in magnitude. The behavior of the attractive eigenvalues is similar for the other potential models.

3 Separable Approximations to the Nucleon-Nucleon Interaction

The Weinberg eigenvalue analysis leads naturally to separable approximations for nucleon-nucleon potentials, which may be of practical interest for solving few-body problems such as four-body scattering [21,22]. The Weinberg eigenstates $\{|\Psi_\nu\rangle\}$ can be used as a basis for a separable representation of the potential [9,15,23,24], with various possible ways to construct such a representation. Here we do not attempt to optimize such an expansion, but focus on the efficacy of a *given* separable expansion as a function of the cutoff, and choose for illustration the expansion in Weinberg eigenvectors at zero energy.

For $E \leq 0$, we use the following separable representation

$$V = \sum_{\nu=1}^{\infty} V |\Psi_{\nu}(E)\rangle \langle \Psi_{\nu}(E)| V, \quad (11)$$

where we choose the normalization of the Weinberg states such that

$$\langle \Psi_{\nu'}(E)|V|\Psi_{\nu}(E)\rangle = \delta_{\nu'\nu}. \quad (12)$$

This separable representation is easily verified by substituting it into the eigenvalue problem, Eq. (6). The T matrix is then given by

$$T = \sum_{\nu=1}^{\infty} \frac{V|\Psi_{\nu}(E)\rangle \langle \Psi_{\nu}(E)|V}{1 - \eta_{\nu}(E)}. \quad (13)$$

As in Refs. [9,15], Eqs. (6) and (13) lead to a sum rule for the exact T matrix at energy E ,

$$\text{Tr} [G_0(E) T(E) G_0(E) T(E)] = \sum_{\nu=1}^{\infty} \frac{1}{(1 - 1/\eta_{\nu}(E))^2}. \quad (14)$$

The summation in the corresponding sum rule to a rank- n approximation $T^{(n)}$ runs only from $\nu = 1$ to $\nu = n$. For $E \leq 0$ each term in the sum is positive definite, so the sum rule is most saturated and the difference between $T^{(n)}$ and T minimized by choosing the n eigenvalues in order of ascending $(1 - 1/\eta_{\nu}(E))^2$. This illustrates a difference between the convergence of the separable expansion and that of the Born series (which depends on the eigenvalues of largest magnitude rather than those closest to unity).

For practical calculations, we can apply the rank- n approximation at fixed energy E to calculate the T matrix at all energies E' . In this case, the analysis of convergence is no longer simply given by the eigenvalues, but we expect the general trends to carry over. Here we choose $E = 0$ and study the accuracy of observables calculated from the eigenvectors corresponding to the n largest eigenvalues, using the representation Eq. (11). As the rank n increases, all eigenvalues that are not included decrease, and thus our expansion improves. In addition, we examine how the rank- n approximation performs as a function of the cutoff, where $V_{\text{low } k}$ is evolved from the Argonne v_{18} potential for all results presented in this section.

In Figs. 11 and 12, the convergence of our truncation is shown by the relative error in the calculated phase shifts for $E_{\text{lab}} = 100$ MeV and 250 MeV (which typify the full range of energies). Our results demonstrate that using a rank- n separable approximation at the particular energy $E = 0$ MeV does reproduce phase shifts reasonably well for $E' \neq E$. Except in a few cases, the convergence

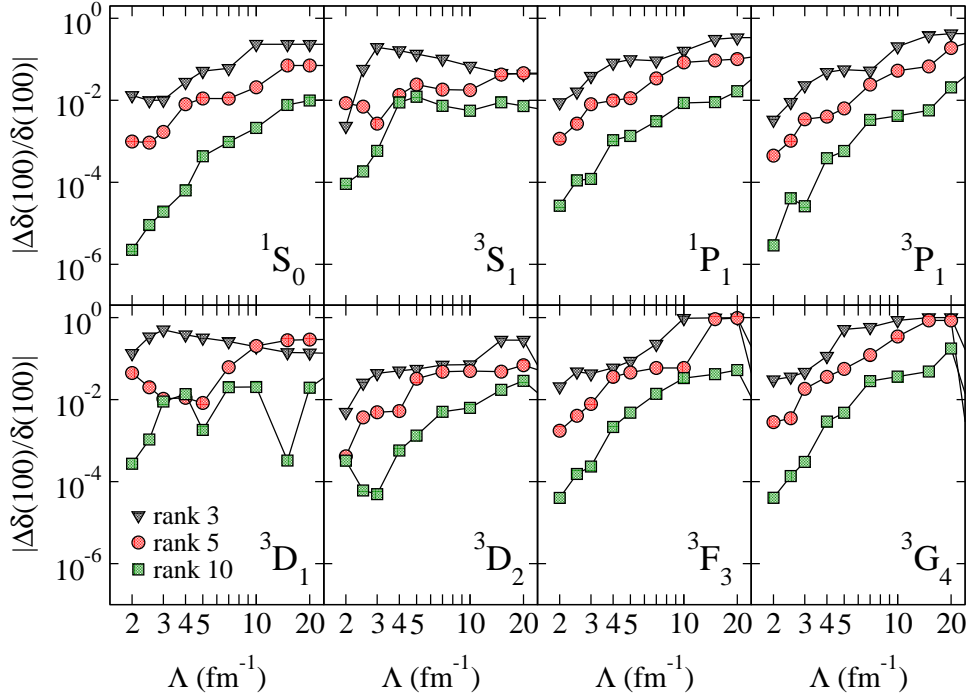


Fig. 11. Relative error in the phase shifts for $E_{\text{lab}} = 100$ MeV as a function of Λ based on separable potentials generated from the Weinberg eigenvectors at $E = 0$ corresponding to the largest $n = 3, 5$ and 10 eigenvalues.

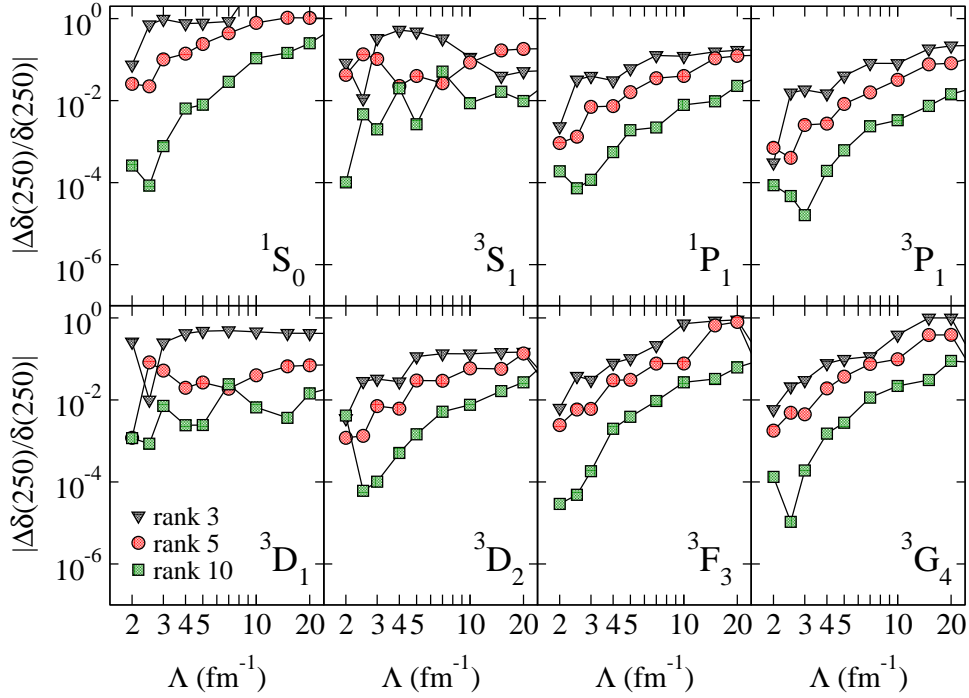


Fig. 12. Relative error in the phase shifts for $E_{\text{lab}} = 250$ MeV as a function of Λ based on separable potentials generated from the Weinberg eigenvectors at $E = 0$ corresponding to the largest $n = 3, 5$ and 10 eigenvalues.

improves monotonically as more terms are included in the separable approximation and, for a particular rank- n approximation, lower cutoffs yield better convergence. As expected, we observe that the convergence is slower in low partial waves where the tensor force is active (3S_1 and 3D_1 in Figs. 11 and 12). Equation (14) implies that the fall-off of Weinberg eigenvalues should be tied to the rate of convergence. This is consistent with Fig. 13, which shows this fall-off in the 1S_0 channel for $E_{\text{lab}} = 100$ MeV.

Further insight into how the convergence varies with the cutoff comes from the predicted triton binding energy. Since we are interested in convergence rather than absolute predictions, we consider for simplicity and convenience the expectation value of the Hamiltonian at each Λ in a basis of harmonic oscillators up to $N_{\text{max}} = 40$ with fixed oscillator parameter $b = 1.7$ fm (that is, the energy is not minimized with respect to this parameter). The result for the triton binding energy E_t with the full potential is compared to results with different rank separable approximations at the same cutoff. The absolute errors are plotted in Fig. 14 as a function of rank for a variety of cutoffs. (Note that full predictions for the triton will vary with the cutoff, because we do not include the Λ -dependent consistent three-body force, but for our purposes this is not relevant.)

At very low rank, the errors are not systematic, but by rank $n = 4$ there is a systematic decrease in the error with decreasing cutoff. Our results can be compared to those from the separable expansions of low-momentum potentials considered in Ref. [25], which used polynomial expansions up to a specified rank. They found as well that calculations of the triton converge to the exact result at lower rank as the cutoff is decreased, with convergence to four digits or better at rank 10, 14 and 20 for $\Lambda = 3, 5$ and 10 fm^{-1} , respectively. Overall, the dramatic improvement in convergence of separable expansions when cutoffs are lowered motivates a future study of how to optimize such expansions. This study should also consider alternative formulations, such as that of Ernst, Shakin and Thaler, which when applied to conventional (and therefore high cutoff) potentials at rank 4, leads to deviations of less than 50 keV for the triton binding energy [26].

In addition to the separable expansion in terms of Weinberg eigenvectors, one can consider a separable inverse scattering approach [15,27] that is based on the scattering phase shifts and does not require a potential model. Here we make a simple exploratory study, using the separable inverse scattering solution for a single channel to compare the inverse scattering low-momentum interaction V_{inv} to $V_{\text{low } k}$ in the S and P-waves. We therefore neglect the coupling of the 3S_1 and 3P_2 channels to the 3D_1 and 3F_2 waves respectively. The generalization to coupled channels and to higher rank separable interactions (such as an attractive and repulsive contribution) is straightforward [27]. For low cutoffs, the perturbative regime with Weinberg eigenvalues $|\eta| < 1$ sug-

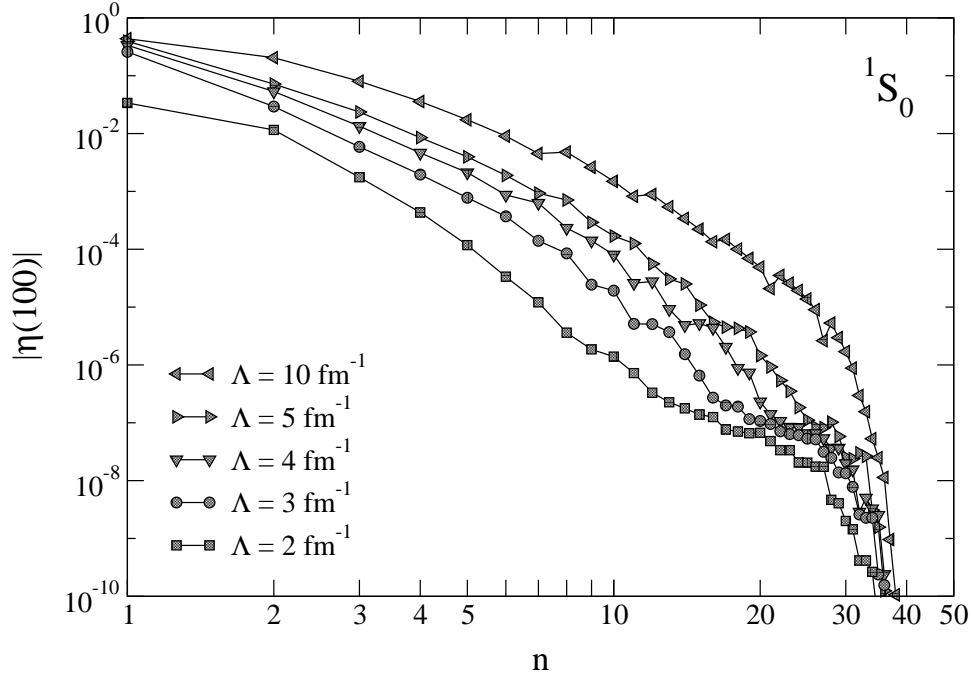


Fig. 13. Magnitude of Weinberg eigenvalues in descending order for the 1S_0 channel at $E_{\text{lab}} = 100$ MeV.

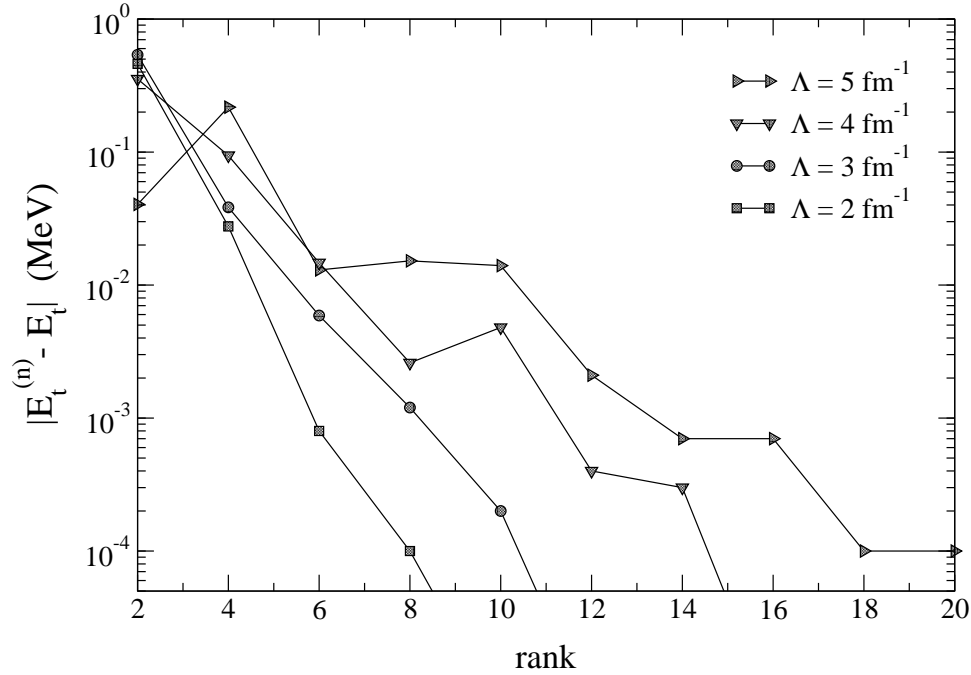


Fig. 14. Absolute error of the triton binding energy for separable expansions of different rank. The results for different cutoffs are obtained in a fixed basis of harmonic oscillators (based only on two-body interactions). The error is with respect to the exact result for the same Λ and model space N_{max} .

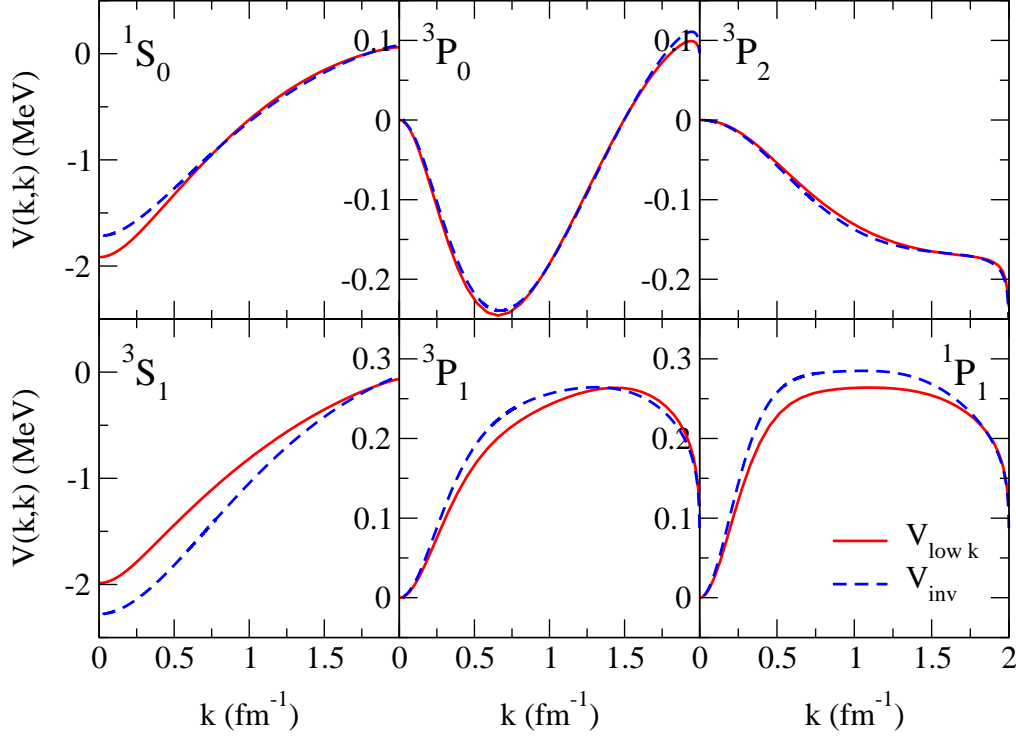


Fig. 15. Diagonal matrix elements $V_{\text{low } k}(k, k)$ compared to separable inverse scattering results $V_{\text{inv}}(k, k)$ for $\Lambda = 2.0 \text{ fm}^{-1}$ in S and P-waves.

gests a direct connection to the phase shifts, except for the S-waves with near-zero-energy bound states. Our results show that the inverse scattering solution may provide a good starting point to make this connection for separable interactions.

For a single channel, the solution to the inverse scattering problem with a one-term separable interaction $V_{\text{inv}}(k, k') = g v(k) v(k')$ is given by (where the sign of g determines the sign of the interaction and $v(k) = \sqrt{V_{\text{inv}}(k, k)/g}$) [15,27]

$$V_{\text{inv}}(k, k) = - \left(\frac{k^2 + k_b^2}{k^2} \right) \frac{\sin \delta(k)}{k} e^{-\Delta(k)}. \quad (15)$$

The factor $(k^2 + k_b^2)/k^2$ is present for channels with a bound state (in the ${}^3\text{S}_1$ partial wave $k_b = \sqrt{m |E_d|/\hbar^2}$ with deuteron binding energy E_d) and

$$\Delta(k) = \frac{2}{\pi} \mathcal{P} \int_0^\Lambda \frac{p dp}{p^2 - k^2} \delta(p). \quad (16)$$

Here we have generalized the conventional inverse scattering solution (where the phase shifts over *all* energies are known) to an effective theory where all phase shifts are known up to the cutoff. Therefore $V_{\text{inv}}(k, k)$ is defined only for momenta $k < \Lambda$.

In Fig. 15, we compare the resulting inverse scattering interaction $V_{\text{inv}}(k, k)$ with $V_{\text{low } k}(k, k)$ for a representative low-momentum cutoff $\Lambda = 2.0 \text{ fm}^{-1}$ in the S and P-waves. We find that the separable inverse scattering solution reproduces qualitatively all features of $V_{\text{low } k}$. The largest differences are observed in the S-waves, which is due to the rank-1 approximation. Note that the (coupled channel) ${}^3\text{P}_2$ partial wave is well described in our single-channel approximation, since the coupling to the ${}^3\text{F}_2$ wave is weak. In addition, the inverse scattering solution leads to the same characteristic dependences close to the cutoff, which makes it clear that these are sharp cutoff artifacts. (Note that the separable inverse scattering solution would go smoothly to zero if one were to modify the phase shifts by a smooth cutoff regulator.) Finally, it is interesting that the single-channel inverse scattering solution leads to a good description of $V_{\text{low } k}$ in channels where the interaction changes from attractive to repulsive, as is the case in the ${}^3\text{P}_0$ partial wave. For low-momentum interactions, where the phase shifts are known over the range of validity of the effective theory, the inverse scattering approach therefore presents a promising addition to separable expansions in Weinberg eigenvectors.

4 Conclusions

In this paper, Weinberg eigenvalues are used as a diagnostic to study the non-perturbative nature of nucleon-nucleon interactions as a function of a momentum cutoff. As the cutoff is lowered using renormalization-group or model-space techniques, the evolution of nonperturbative features at large cutoffs from strong short-range repulsion and iterated tensor interactions are monitored via the repulsive complex Weinberg eigenvalues. Major decreases in the magnitudes of repulsive eigenvalues are observed for all conventional potentials when evolved to low momentum, even though two-body observables are unchanged.

When all eigenvalues for a given channel lie within the unit circle, the T matrix expansion in terms of the potential V is perturbative in that channel, with the magnitude of the largest eigenvalues setting the rate of convergence. The repulsive eigenvalues satisfy this criterium in all channels for cutoffs of 2 fm^{-1} , where the crossover from the nonperturbative ($|\eta| > 1$) to the perturbative regime ($|\eta| < 1$) happens for $\Lambda > 3 \text{ fm}^{-1}$. The largest attractive eigenvalues, however, remain close to or beyond the unit circle in the S-waves, because they are due to the bound or nearly bound states. Consequently, this is the only surviving source of nonperturbative behavior for the Born series with low-momentum interactions. As shown in Ref. [5], the large attractive eigenvalues decrease rapidly due to Pauli blocking as the density is increased toward saturation density. This opens the possibility of perturbative and therefore systematic calculations of nuclear matter.

Chiral EFT interactions are also low-momentum interactions and are expected to be soft. However, at N³LO the isoscalar central part of the sub-sub-leading 2 π -exchange interaction is strongly repulsive at short distances [20]. This leads to large repulsive Weinberg eigenvalues for N³LO potentials in both singlet and triplet channels. As a result of these nonperturbative features at N³LO, the S-wave component of the deuteron wave function [14] has a short-range part that is similar to what is found with a repulsive core. In addition, the tensor force, e.g., from pion exchange, is singular at short distances. We have found major decreases of the repulsive Weinberg eigenvalues as the cutoff is run down from $\Lambda = 3 \text{ fm}^{-1}$ to 2 fm^{-1} , which tames the impact of the tensor force and of the nonperturbative features at N³LO. This motivates the evolution of chiral interactions to lower cutoffs to improve their effectiveness for few- and many-body problems [5,8].

The decrease of the Weinberg eigenvalues implies that separable expansions of nuclear interactions become more effective for lower cutoffs. This was demonstrated for NN scattering and the triton binding energy: for cutoffs of 2 fm^{-1} , the typical relative error in the NN phase shifts is 0.1%, and the convergence to the exact triton binding energy is to four digits at rank 6, 10, 12 and 14 for $\Lambda = 2, 3, 4$ and 5 fm^{-1} , respectively. Such separable expansions may be useful for four-body scattering [21,22] or to develop microscopic interactions that can be handled by the current methods in nuclear reaction theory. Perturbative Weinberg eigenvalues also suggest a closer connection of low-momentum interactions to phase shifts. This was explored with rank-1 separable inverse scattering solutions, which were found to qualitatively reproduce the momentum dependences of $V_{\text{low } k}$.

Acknowledgements

We thank Andreas Nogga for useful discussions, and Evgeny Epelbaum for providing us with his code for the N²LO and N³LO potentials. This work was supported in part by the National Science Foundation under Grant No. PHY-0354916 and the US Department of Energy under Grant No. DE-FG02-97ER41014.

References

- [1] S.K. Bogner, T.T.S. Kuo, A. Schwenk, D.R. Entem and R. Machleidt, Phys. Lett. **B576** (2003) 265.
- [2] S.K. Bogner, T.T.S. Kuo and A. Schwenk, Phys. Rept. **386** (2003) 1.

- [3] S.K. Bogner, A. Schwenk, T.T.S. Kuo and G.E. Brown, nucl-th/0111042.
- [4] A. Nogga, S.K. Bogner and A. Schwenk, Phys. Rev. **C70** (2004) 061002(R).
- [5] S.K. Bogner, A. Schwenk, R.J. Furnstahl and A. Nogga, Nucl. Phys. **A763** (2005) 59.
- [6] S.K. Bogner and R.J. Furnstahl, Phys. Lett. B **632** (2006) 501.
- [7] S.K. Bogner and R.J. Furnstahl, nucl-th/0602017.
- [8] S.K. Bogner, R.J. Furnstahl, S. Ramanan and A. Schwenk, in preparation.
- [9] S. Weinberg, Phys. Rev. **131** (1963) 440.
- [10] R.B. Wiringa, V.G.J. Stoks and R. Schiavilla, Phys. Rev. **C51** (1995) 38.
- [11] R. Machleidt, Phys. Rev. **C63** (2001) 024001.
- [12] V.G.J. Stoks, R.A.M. Klomp, C.P.F. Terheggen and J.J. de Swart, Phys. Rev. **C49** (1994) 2950.
- [13] D.R. Entem and R. Machleidt, Phys. Rev. **C68** (2003) 041001(R).
- [14] E. Epelbaum, W. Glöckle and U.G. Meißner, Nucl. Phys. **A747** (2005) 362.
- [15] G.E. Brown and A.D. Jackson, *The Nucleon-Nucleon Interaction* (North-Holland, New York, 1976).
- [16] M. Scadron and S. Weinberg, Phys. Rev. **133** (1964) 1589.
- [17] W. Gloeckle, *The Quantum Mechanical Few-Body Problem* (Springer-Verlag, New York, 1983).
- [18] G.E. Brown, *Unified Theory of Nuclear Models and Forces* (North-Holland, Amsterdam, 1971).
- [19] E. Epelbaum, W. Glöckle and U.G. Meißner, Eur. Phys. J. **A19** (2004) 401.
- [20] N. Kaiser, Phys. Rev. **C64** (2001) 057001.
- [21] R. Lazauskas, J. Carbonell, A.C. Fonseca, M. Viviani, A. Kievsky and S. Rosati, Phys. Rev. **C71** (2005) 034004.
- [22] A. Nogga *et al.*, nucl-th/0602003.
- [23] G.H. Rawitscher and L. Canton, Phys. Rev. **C44** (1991) 60.
- [24] L. Canton and G.H. Rawitscher, J. Phys. **G17** (1991) 429.
- [25] H. Kamada, S. Fujii, E. Uzu, M. Yamaguchi, R. Okamoto and Y. Koike, nucl-th/0510073.
- [26] W. Schadow, W. Sandhas, J. Haidenbauer and A. Nogga, Few-Body Sys. **28** (2000) 241.
- [27] F. Tabakin, Phys. Rev. **177** (1969) 1443.